Analysis of Recent Extreme Events Measured by the Barotropic Component of the Atmosphere

H.L. TANAKA

Froutier Research Center for Global Change, Tokyo, Japan
Geoenvironmental Sciences, University of Tsukuba, Tsukuba, Japan

and

Mio MATSUEDA

Graduate School of Life and Environmental Sciences, University of Tsukuba, Tsukuba, Japan

(Manuscript received 4 January 2004, in final form 12 May 2004)

Abstract

In this study, recent extreme events over the Northern Hemisphere are quantified in terms of an energy norm of the anomaly of the state variables. Since persistent low-frequency variabilities are characterized, in most cases, by their barotropic structure, the energy norm of the anomaly is measured for the barotropic component of the atmosphere. The norm is then normalized by its climatology to assess the abnormality of the extreme events. In this study the norm is evaluated in the framework of the 3-D spectral primitive equation model to assess the external forcing as well as the state variabiles.

According to the analysis of the monthly mean anomaly data for 50 years from 1953 to 2002, the most abnormal months appear to be Apr. 1997, Jan. 1963, Jan. 1977, Mar. 1983, Apr. 1967, Feb. 1989, and Jan. 1989. Those are well known abnormal months in the past studies. In this study, the top 3% of the extreme events are listed as the abnormal months.

The quantification of the abnormality is further extended to the external forcing of the barotropic component of the atmosphere and also to the SST anomaly. It is found that only 3 cases of the abnormal months (Jan. 1963, Feb. 1989 and Jan. 1989) are associated with the abnormal external forcing, and the rest of the abnormal months are associated with the non-abnormal external forcing. Likewise, it is found that most of the abnormal external forcing result in a non-abnormal month. The SST forcing anomaly is not directly related to the external forcing. It is concluded from the result that more than 80% of the abnormal months are induced by the natural variability of the barotropic component of the atmosphere under the non-abnormal external forcing for the last 50 years. For the monthly time scale, the chaotic nonlinear behavior is quantitatively larger than a linear response to the external forcing or that to the SST anomaly.

1. Introduction

Analysis of atmospheric extreme events (abnormal weather) is a great concern in the climate change as well as in the medium to long-range weather forecasing. Knowing the direct and indirect causes of the abnormal weather would lead to the improvement of the long-range forecasting and to the understanding of the climate change (see IPCC 2001). However, in most cases, the reasons of the abnormal weather or any extreme event are hidden by the complexity of the chaotic nature of the non-

Corresponding author: Hiroshi L. Tanaka, Geoenvironmental Sciences, University of Tsukuba, Tsukuba 305-8572, Japan.
E-mail: tanaka@sakura.cc.tsukuba.ac.jp

linear fluid dynamics (see JMA 1994; 1999). The abnormal weather is often explained, for example, by the occurrence of blocking high or an amplified planetary waves which meanders the upper-air jet stream with abnormal ridges and troughs. The true dynamical reason why the jet stream has meandered is beyond the scope of the analysis. If there is a pronounced phenomenon such as El Niño or La Niña, the direct cause of the abnormal weather is attempted to link with them using the analysis of quasi-stationary Rossby wave-train (Bell and Halpert 1998; Bell et al. 1999; Kushnir et al. 2002; Peng et al. 2003). If there is a major volcanic eruption, the abnormal weather is attempted to explain with them by the analysis of radiative impact to the atmosphere (Kawamata et al. 1992; Graf et al. 1994). However, if there is no such obvious impact of external forcing on the atmosphere, the abnormal weather would be elucidated as a natural variability contained in the chaotic nonlinear fluid mechanics, and the true direct and indirect causes are something of an enigma (see Namias 1978; Branstator 1990; Yasunari 1997; Frederiksen and Branstator 2001; Kravtsov et al. 2003; Branstator and Frederiksen 2003; Tanaka 2003a).

We wonder if the long-range forecasting for the future would be possible even without knowing the true causes for the past abnormal weather. It may therefore be an important research subject to understand to what extent the abnormal weather is explained by the natural variability of the atmosphere, or by the external abnormal forcing.

According to the analysis by Tanaka (2003a), most of the extreme events are induced by the low-frequency variabilities of the atmosphere such as blocking high, Arctic Oscillation (AO) and PNA-like teleconnections, which are characterized by their barotropic structure (Wallace and Blackmon 1981; Wallace and Gutzler 1981; Thompson and Wallace 1998; Tanaka 1998). Therefore, the dynamical understanding of those low-frequency variabilities may be the central subject for long-range weather forecasting. The dynamical role of the barotropic component of the atmosphere is extensively investigated by Tanaka (1985; 1998; 2003b). According to the result of the 3-D spectral energetics analysis, any heat related baroclinic energy (available potential energy) is converted to barotropic energy when the baroclinicity is removed by the activity of the synoptic disturbances. It is quite natural because synoptic disturbances are exited by baroclinic instability to remove the baroclinicity.

The barotropic component of the atmosphere is dynamically unique in that it consists of an isolated discrete spectrum with respect to the vertical normal mode, while all other baroclinic components construct a continuous spectrum. In this respect, we may regard the barotropic component as a physical mode of the atmosphere. Atmospheric energy is transformed to the discrete spectrum of the barotropic mode in nature by the baroclinic instability at the synoptic scale. Interestingly, the accumulated barotropic energy at the synoptic eddies is then transformed to planetary waves by the up-scale energy cascade under the constraint of the 2-D fluid dynamics (Kraichnan 1967; Tung and Orlando 2003). It is in this process when the low-frequency variabilities of amplified planetary waves cause extreme events over the hemispheric scale. When the up-scale energy cascade amplifies the planetary waves, a blocking occurs by the Rossby wave breaking (Tanaka 1998); and the Arctic Oscillation is excited when the up-scale energy cascade reaches to the zonal wavenumber 0 (Tanaka 2003b). Many of the extreme events can be induced by the internal natural variability of the barotropic component of the atmosphere without a specific external forcing as documented by Branstator (1990) and Frederiksen and Branstator (2001). Hence, we can investigate the cause of the abnormal weather within the framework of the natural variability of the 2-D fluid dynamics or of the abnormal external forcing to the barotropic component of the atmosphere.

The purpose of the present study is to analyze the recent extreme events using a quantitative abnormality index for the barotropic component of the atmosphere over the Northern Hemisphere. We attempt to separate the cause of the extreme events in a natural variability of the 2-D fluid dynamics and/or a forced response to the external forcing of the barotropic component of the atmosphere. A possible link to the SST anomaly is also investigated.

In section 2, the governing barotropic model equations and the data used in this study are

described. In section 3, some examples of anomaly distributions are presented for the barotropic component of the atmosphere, the external forcing, and the SST of the same month. The abnormality index is then introduced in section 4 to quantify the magnitude of the respective anomalies. The long-term time series of the respective abnormality indices are compared with each other to investigate the possible cause of each extreme event. Finally, in section 5, the dynamical cause of the extreme events is discussed in the framework of the natural variability or the external forcing to the barotropic component of the atmosphere.

2. Analysis method and data

2.1 Analysis method

The analysis method is based on the barotropic P-model described in Tanaka and Nohara (2001), where the external forcing of the barotropic model is evaluated as the residual of the governing equation. A brief description of the barotropic P-model is presented here.

A system of primitive equations with a spherical coordinate of longitude λ, latitude θ, pressure p, and time t may be reduced to three prognostic equations of horizontal motions and thermodynamics for three dependent variables of $U = (u, v, \phi')^T$. Here, u and v are the zonal and meridional components of the horizontal velocity, respectively, and ϕ' is a departure of the local isobaric geopotential from the reference state geopotential ϕ_0. The superscript T denotes a transpose. Using a matrix notation, these primitive equations may be written as

$$\mathbf{M}\frac{\partial U}{\partial t} + \mathbf{L}U = N + F, \tag{1}$$

where the left-hand side of (1) represents linear terms with matrix operators $\mathbf{M}$ and $\mathbf{L}$ and the dependent variable vector U. Refer to Tanaka (1998) for the definition of matrices $\mathbf{M}$ and $\mathbf{L}$. The right-hand side represents a nonlinear term vector N and a diabatic term vector F, which includes the zonal and meridional components of frictional forces and diabatic heating rate.

In order to obtain a system of 3-D spectral primitive equations, the vectors U and F are expanded in 3-D normal mode functions in a resting atmosphere, $\Pi_{nlm}(\lambda, \theta, p)$:

$$U(\lambda, \theta, p, t) = \sum_{nlm} w_{nlm}(t) X_m \Pi_{nlm}(\lambda, \theta, p), \tag{2}$$

$$F(\lambda, \theta, p, t) = \sum_{nlm} f_{nlm}(t) Y_m \Pi_{nlm}(\lambda, \theta, p), \tag{3}$$

where the dimensionless expansion coefficients $w_{nlm}(t)$ and $f_{nlm}(t)$ are the functions of time alone. These may be computed by the inverse Fourier transforms of U and F from the physical domain.

$$w_{nlm}(t) = \langle U(\lambda, \theta, p, t), X_m^{-1}\Pi_{nlm}(\lambda, \theta, p)\rangle, \tag{4}$$

$$f_{nlm}(t) = \langle F(\lambda, \theta, p, t), Y_m^{-1}\Pi_{nlm}(\lambda, \theta, p)\rangle. \tag{5}$$

The subscripts represent zonal wavenumbers n, meridional indices l, and vertical indices m. The scaling matrices should be defined for each vertical index as:

$$X_m = diag(c_m, c_m, c_m^2), \tag{6}$$

$$Y_m = diag(2\Omega c_m, 2\Omega c_m, 2\Omega), \tag{7}$$

where $c_m = \sqrt{gh_m}$ is a phase speed of gravity waves in shallow water associated with the equivalent height h_m, Ω is the angular speed of the earth's rotation, and *diag* represents diagonal matrix. The expansion basis of the 3-D normal mode functions $\Pi_{nlm}(\lambda, \theta, p)$ is obtained as an eigensolution of a homogeneous partial differential equation, putting zero on the right-hand side of (1). The 3-D normal mode functions are given by a tensor product of vertical structure functions and Hough harmonics associated with the linear operators $\mathbf{M}$ and $\mathbf{L}$, respectively (Kasahara 1976, 1978). They form a complete set and satisfy an orthonormality condition under a proper inner product $\langle , \rangle$ representing the global mass integral.

By expanding those variables in 3-D normal mode functions, a system of 3-D spectral primitive equations are obtained in terms of the spectral expansion coefficients:

$$\frac{dw_i}{d\tau} + i\sigma_i w_i = -i\sum_{jk} r_{ijk} w_j w_k + f_i, \quad i = 1, 2, 3, \ldots \tag{8}$$

where τ is a dimensionless time scaled by $(2\Omega)^{-1}$, σ_i is the eigenfrequency of the Laplace's tidal equation, and r_{ijk} is the interaction coefficients for nonlinear wave-wave interactions calculated by the triple products of the 3-D normal mode functions. The triple subscripts

are shortened for simplicity as $w_{nlm} = w_i$. There should be no confusion in the use of i for a subscript, even though it is used for the imaginary unit in (8).

In the 3-D spectral representation, the vertical expansion basis functions may be divided into barotropic $(m = 0)$ and baroclinic $(m \neq 0)$ components. We may construct a simple spectral barotropic model, using only the barotropic components $(m = 0)$ of the Rossby modes, by truncating all the baroclinic modes and high-frequency gravity modes (see Kasahara 1977). Such a model is equivalent to that predicting the vertical average of meteorological variables. The barotropic components capture the essential features of the low-frequency variability of planetary-scale motions. The spectral equation for such a barotropic model may be written as:

$$\frac{dw_i}{d\tau} + i\sigma_i w_i = -i \sum_{jk} r_{ijk} w_j w_k + s_i,$$

$$i = 1, 2, 3, \ldots, (m = 0), \tag{9}$$

where the indices of the subscripts run only for the barotropic modes. The zonal and meridional wave truncation of the present model is equivalent to rhomboidal 20 with an equatorial wall. The degree of freedom of the system is reduced enormously by these truncations. The spectral equation for such a barotropic model (9) has the same form as for the baroclinic model equation (8), except for the fact that the barotropic-baroclinic interaction appears on the right hand side, which has been included in s_i. According to the observational analysis by Tanaka (1985), the barotropic-baroclinic interaction dominates the physical external forcing (mostly frictional force and viscosity) for the barotropic component. Henceforth, s_i is designated as the external forcing of the barotropic component of the atmosphere. The atmospheric variability is caused by the natural variability due to the linear and nonlinear terms and by the external forcing s_i in (9).

2.2 Data

The data used in this study are four-times daily NCEP/NCAR reanalysis for 50 years from 1953 to 2002 (see Kalnay et al. 1996). The data contain horizontal winds $V = (u, v)$ and geopotential ϕ, defined at every 2.5° longitude by 2.5° latitude grid points over 17 mandatory vertical levels from 1000 to 10 hPa.

The expansion coefficients w_i are obtained by the Fourier transform of (4) from the dataset of $U = (u, v, \phi')^T$. The atmospheric anomaly is assessed only for the Northern Hemisphere by the symmetric extension of the northern data to the Southern Hemisphere. In order to evaluate the external forcing s_i, the state variable w_i is interpolated to the model's time step of one hour by cubic spline method. The external forcing s_i is then diagnostically calculated from w_i as the residual of the equation (9). Since the dynamical part of primitive equations are accurate within at most 1% error, the external forcing s_i should have the same order as the analysis error in w_i. Considering the fact that w_i is the vertical mean of the observed and analyzed state variables, the accuracy is higher than the typical value of the observation error and analysis error by the argument of the standard error of the mean. We may thus regard that s_i is evaluated quite accurately to conduct the analysis of this study.

Using the long-term history data of w_i and s_i, the monthly mean climate of $\tilde{w}_i$ and $\tilde{s}_i$ and its anomaly of w_i' and s_i' are constructed for the subsequent analysis. There are a total of 600 samples for 50 years of monthly data. The separation of the continuous atmospheric data in monthly mean of the calender year is not physical but rather conventional. Yet, the statistical features of the extreme events should not change much for large sample of the data.

In this study, we used the Extended Reconstructed Sea Surface Temperature (ERSST) dataset (see Smith and Reynolds 2003) in order to compare with the external forcing of the barotropic component of the atmosphere. The ERSST data are given on the 2.0° longitude by 2.0° latitude grids for the monthly mean from January 1953 to December 2002. Since the quality of the SST data before 1979 is questionable due to the lack of satellite observations, discussion is restricted for the period from 1979 to 2002 over the SST domain from 60°S to 60°N. Any grid occupied by ice is removed from the analysis.

3. Distributions of anomalies

3.1 Extreme event in January 1963

January 1963 is known as one of the most abnormal months which occurred in the North-

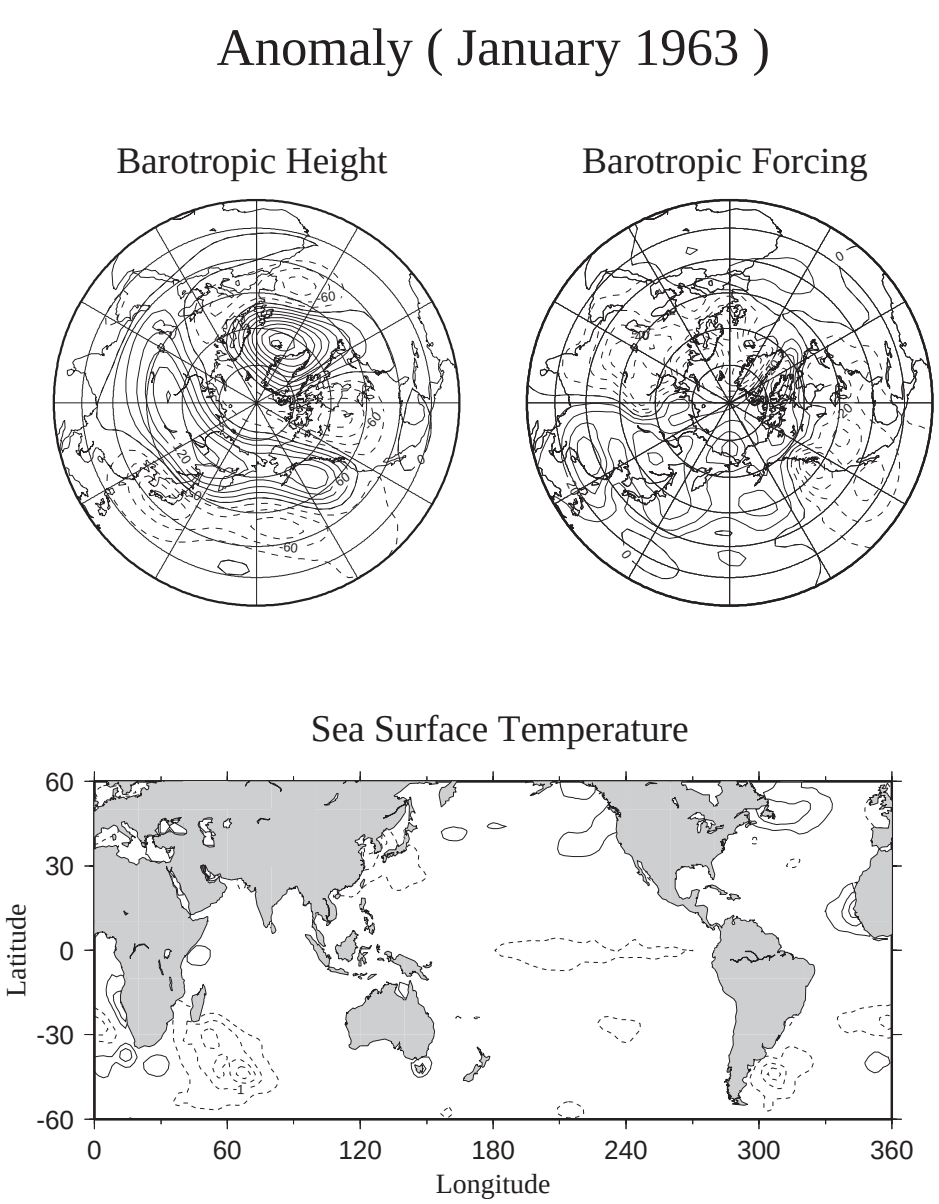

Fig. 1. The distributions of (a: upper left) the barotropic height anomaly and (b: upper right) the barotropic forcing anomaly over the Northern Hemisphere and (c: lower center) the corresponding SST anomaly for January 1963. The contour intervals are in 30 m, 10 ($\times 10^{-3}$) m s^{-1} and 0.5 K, respectively.

ern Hemisphere (see Wiin-Nielsen and Drake 1965; Wiin-Nielsen 1967).

Figure 1a illustrates the height anomaly of the barotropic component of the atmosphere over the Northern Hemisphere (hereafter referred to as barotropic height). The monthly mean anomaly of w_i in (9) is converted to the geopotential height by means of the Fourier transform in (2) to present the height anomaly. Wind anomaly can be analyzed by the same Fourier transform, but the distribution is closely in a geostrophic balance because the gravity modes are eliminated in the analysis. A positive height anomaly of 240 m is located at Iceland. Another positive anomaly of 150 m is seen at Siberia extending toward the Gulf of

Alaska. Negative anomalies of −90 m are seen at Japan, central Canada, and the Azores.

The hemispheric distribution of the external forcing to the barotropic height is shown in Fig. 1b (hereafter referred to as barotropic forcing). The monthly mean anomaly of s_i in (9) is converted to the external height forcing by means of the Fourier transform in (2). Negative and positive forcing anomalies over the western and eastern half of the Eurasian continent, respectively, imply a reduced topographic forcing associated with the Tibettern Plateau. The magnitude is of the order of 40 (units are 10^{-3} m s^{-1}). There is no marked positive forcing around Iceland, suggesting that the large positive height anomaly in Fig. 1a is not produced by the local response to the external forcing. The distribution of the SST anomaly for the same month is presented in Fig. 1c. The result shows no noticeable anomaly in the SST. From this result, the abnormal weather in Fig. 1a and the abnormal external forcing in Fig. 1b are unlikely to be explained by the boundary forcing due to the SST anomaly.

3.2 *Extreme event in January 1977*

January 1977 was extreme in that an abnormal high pressure system stayed in the Arctic for a month (Namias 1978). A marked climate shift has occurred after this extreme event as the realization of the Pacific Decadal Oscillation (PDO). This shift had repercussions throughout the high latitudes of the North Pacific (see Kashiwabara 1987; Nitta and Yamada 1989; Trenberth 1990; Trenberth and Hurrell 1994; Graham 1994).

Figure 2a illustrates the barotropic height anomaly for the month. A positive height anomaly of 420 m is located in the Arctic Ocean. The magnitude of the height anomaly is the most extreme in the historical record in the Northern Hemisphere. A negative anomalies of −180 m is seen at the Aleutian and another one at England. The anomaly pattern corresponds to the negative AO index (Thompson and Wallace 1998; Tanaka 2003b).

The distribution of the barotropic forcing in Fig. 2b shows negative anomalies of 30 units at Siberia and the West Coast of the US. Localized positive anomalies of 30 units are seen at north Pacific and Atlantic. The magnitude of the forcing anomaly is weaker than that in Fig. 1b. The distribution of the SST anomaly in Fig. 2c shows a typical El Niño pattern at the equatorial Pacific with the peak value of 1.5 K. The result suggests some connection between the SST anomaly and the extreme event over the north Pacific and the Arctic Ocean through the characteristic forcing pattern induced by the PDO. Yet, the speculation is inconclusive. The extreme event during the winter of 1977 is known to trigger the climate shift from the positive to negative AO regimes.

3.3 *Extreme event in January and February 1989*

The abnormal weather in January and February 1989 was extensively documented by Walsh and Chapman (1990), and the comprehensive heat budget analysis was conducted by Tanaka and Milkovich (1990). The monthly mean temperature at Barrow Alaska was negative in January by 3σ while that in February was positive by 4σ, where σ denotes the standard deviation of the monthly mean temperature variation. The normal probability of the 4σ corresponds to one in 10,000 events.

Figure 3a illustrates the barotropic height anomaly for January 1989. A negative height anomaly of 270 m occupies the Arctic region, and positive height anomalies of 150 m are seen at the Europe and the north Pacific. The anomaly pattern corresponds to the typical positive AO index.

The distribution of the barotropic forcing in Fig. 3b shows positive and negative forcing anomalies over the western and eastern flank of the Tibettern Plateau, respectively, which implies an intensified topographic forcing just opposite to the case in Fig. 2b. The magnitude is of the order of 40 units. The distribution of the SST anomaly in Fig. 3c shows a typical La Niña pattern at the equatorial Pacific with the peak value of −2.5 K.

Figure 4a illustrates the same distribution for subsequent February. The height anomaly shows similar positive AO index pattern except for the pronounced positive height anomaly at the West Coast of the US. During almost a month, a series of blocking highs were created around Alaska to cause an abnormally warm spell. A heat budget analysis for the abrupt shift from the cold spell to warm spell in Alaska was reported by Tanaka and Milkovich

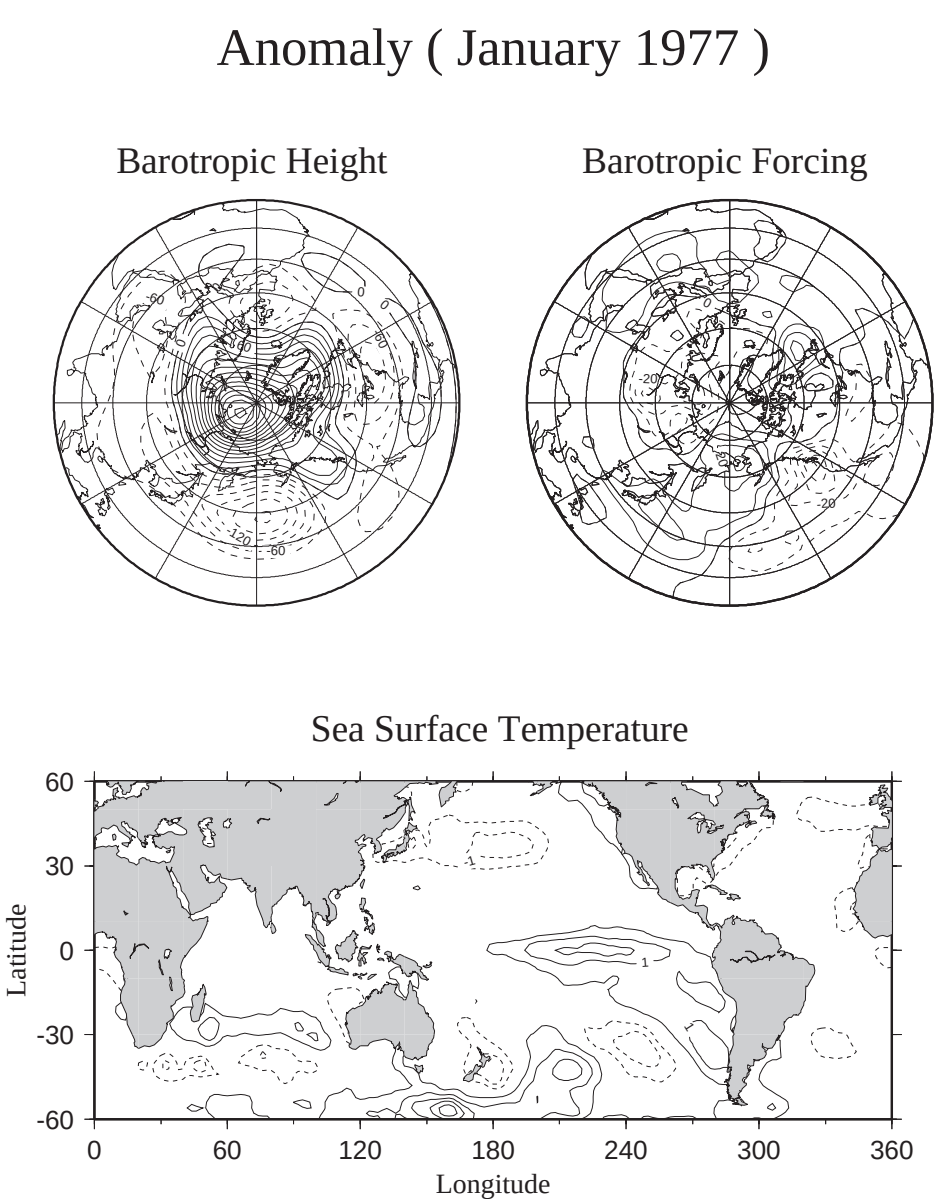

Fig. 2. Same as Fig. 1, but for January 1977.

(1990), indicating the persistent adiabatic warming due to the downward motion associated with the formation of a blocking high over Alaska.

The distribution of the barotropic forcing in Fig. 4b shows similar topographic forcing pattern at the Eurasian continent. A notable positive forcing anomaly is seen at the north of Alaska, which explains the direct positive forcing of the positive height anomaly in Fig. 4a. The magnitude is of the order of 40 units. Figure 4c illustrates the distribution of the SST anomaly in February with a typical La Niña pattern as shown in Fig. 3c. The equatorial SST anomaly is slightly reduced to −2.0 K.

It is noteworthy that the same La Niña pattern has resulted in an extreme cold January and an extreme warm February in Alaska. The result suggests a complicated atmospheric response to the SST anomaly which is not explained by a simple linear theory. The extreme event during the winter of 1989 is known to

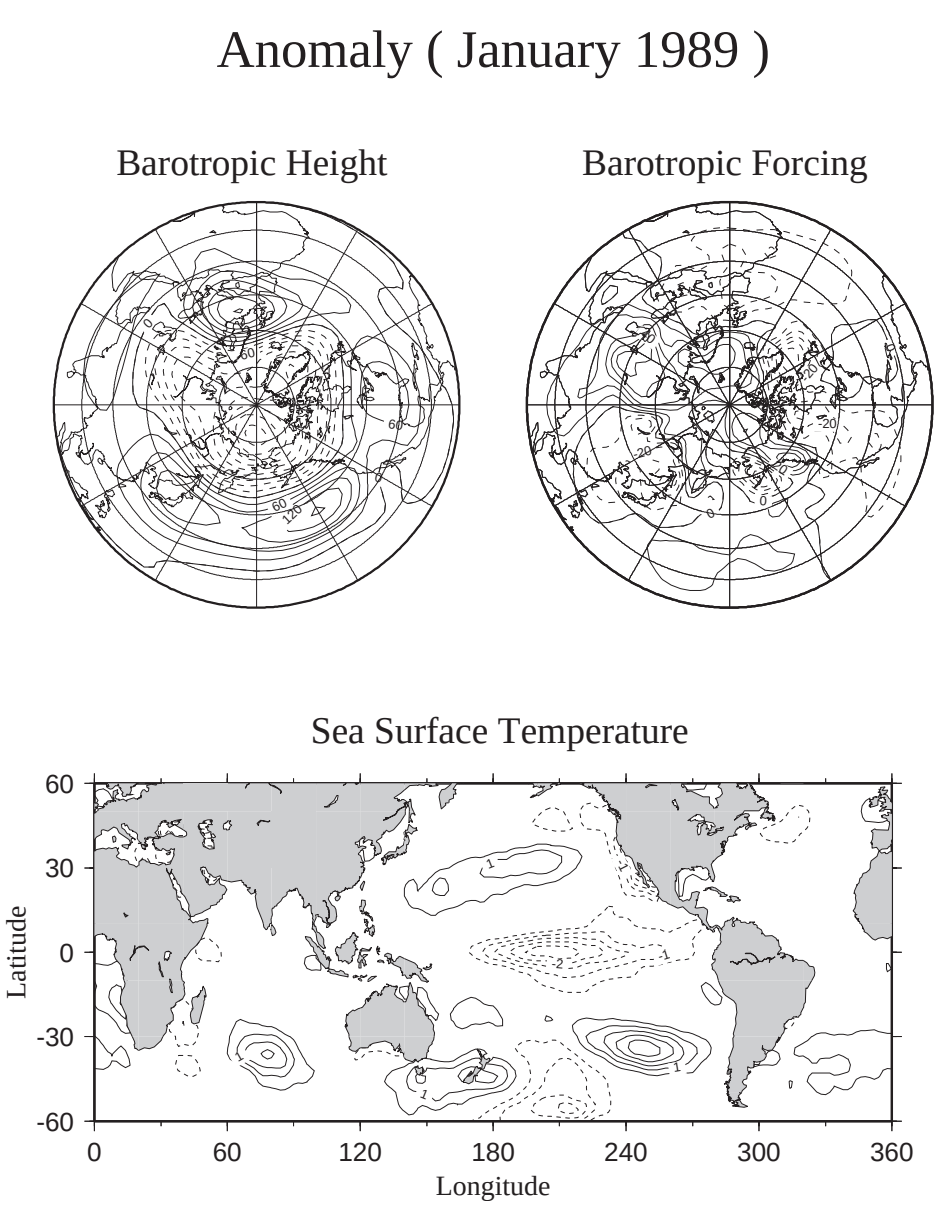

Fig. 3. Same as Fig. 1, but for January 1989.

have triggered the climate shift from the negative AO to positive AO regimes.

3.4 Extreme event in April 1997

Finally, an example of abnormal weather in Spring is presented here. In general, the atmospheric anomaly is larger in winter than in summer. Some normalization is necessary to compare the magnitude of anomaly in different seasons. April 1997 was a typical case of an exceptionally large anomaly for this season. A persistent polar night vortex in March resulted in the nonantecedent ozone hole in the Northern Hemisphere. The strong westerly wind event in the tropics has triggered the onset of the largest El Niño in this century (Bell and Halpert 1998; JMA 1999; Lengaigne et al. 2003).

Figure 5a illustrates the barotropic height anomaly for April 1997. A negative height anomaly of 210 m occupies the Arctic region extending to the Mediteranean and to the north

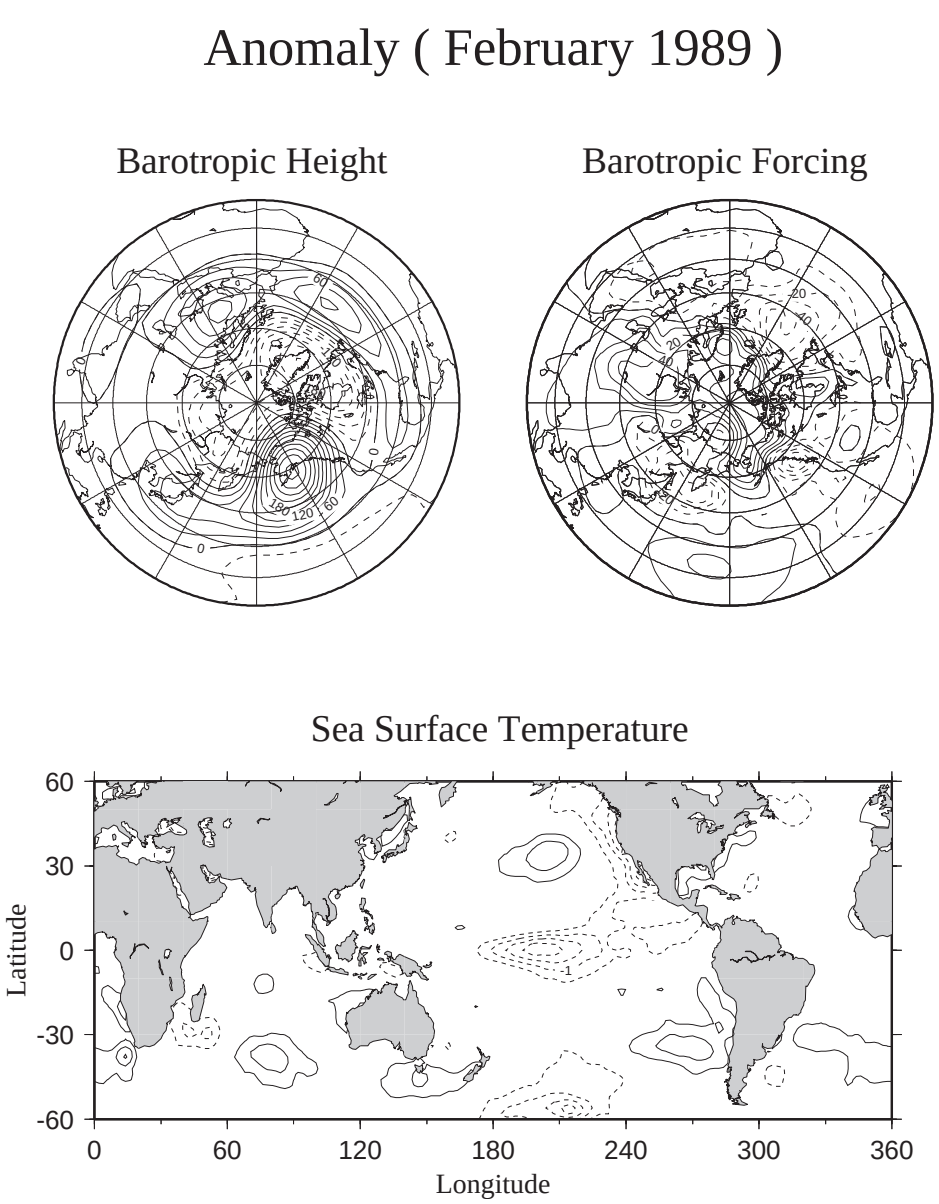

Fig. 4. Same as Fig. 1, but for February 1989.

Pacific. Positive height anomalies of 120 m are seen at the north Atlantic and Siberia. The opposite signs of anomaly at the north Pacific and Atlantic is similar to the second EOF pattern in the Northern Hemisphere as documented by Tanaka (2003b).

The distribution of the barotropic forcing in Fig. 5b shows positive and negative forcing anomalies over Europe and west Siberia with the magnitude of 40 units. The forcing is out of phase with that in the height pattern, and tends to damp the anomaly. Thus, the anomaly ought to be excited by the nonlinear dynamical process internal to the atmosphere in (9). The distribution of the SST anomaly in Fig. 5c illustrates the beginning of the El Niño event during 1997/1998. It is interesting to note that an abnormal height pattern took place in April 1997 just before the beginning of the largest El Niño event in this century. Although the magnitude of the anomaly is comparable with that in the winter season, the abnormality index (see the next section) of this month turns out to be the largest in the recent 50 years.

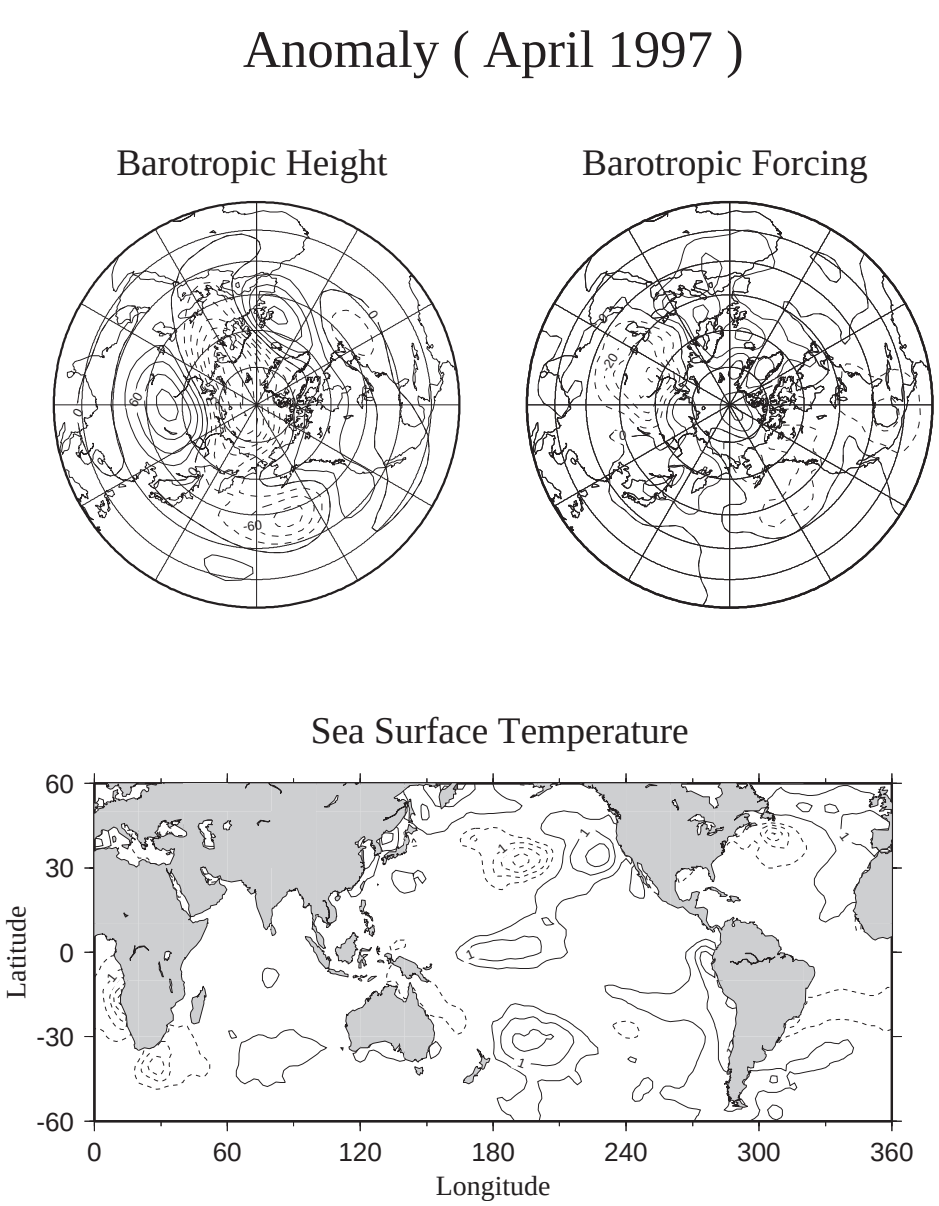

Fig. 5. Same as Fig. 1, but for April 1997.

4. Abnormality indices

4.1 Anomaly norm for the atmosphere

In this section, the abnormality of the anomaly in the barotropic atmosphere presented in section 3 is quantified to assess the relative magnitude of the anomaly. One of the reasonable quantifications of the intensity of the anomaly over the hemisphere may be calculating the variance of the anomaly over the analysis domain.

As discussed by Tanaka (2003b), total energy E of the atmosphere (sum of kinetic energy and available potential energy) is simply the sum of the energy elements E_i defined by:

$$E_i = \frac{1}{2} p_s h_m |w_i|^2, \tag{10}$$

where w_i is the state variable in (9), p_s is the mean surface pressure, and h_m is the equivalent depth of the vertical mode m. The value must be divided by 2 for zonal components. The magnitude of the atmospheric anomaly can be

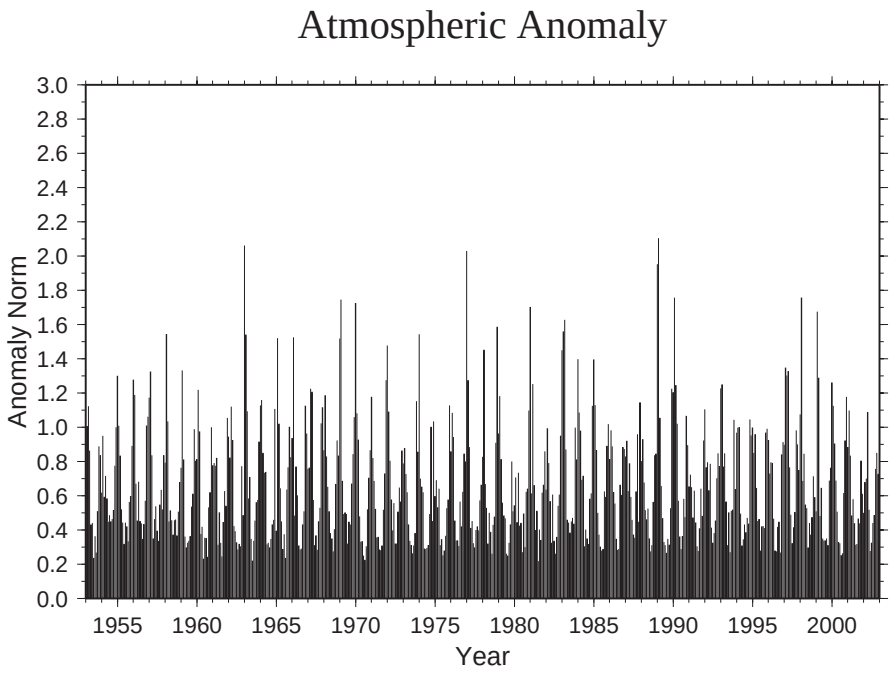

Fig. 6. The anomaly norm of the barotropic component of the atmosphere E_A (10^{-4}) for 1953 to 2002.

measured by the same energy norm replacing w_i by its anomaly w_i'. Since only the barotropic component $(m = 0)$ is considered in this study, the scaling parameters of $p_s h_m$ are disregard for simplicity and define the 2-norm of the atmospheric anomaly E_A by the following dimensionless form:

$$E_A = \sum_i \frac{1}{2} |w_i'|^2, \tag{11}$$

where the summation is taken over the all state variables. The anomaly norm is calculated for the monthly mean data, so the contributions from transient eddies are not included. The anomaly norm describes the global features of the magnitude of the anomaly and is zero only when the atmosphere is identical to the climate. Since the abnormal weather is often assessed in the regional framework, a care must be taken to use the global index defined in this study.

Figure 6 shows the time series of the atmospheric anomaly norm E_A for 1953 to 2002. In this plot, the magnitude of the anomaly in section 3 is quantified by the energy norm in (11). If the values are multiplied by $p_s h_m (\sim 10^9)$, the units become J m^{-2}. Note that not only the height variance (available potential energy) but also the wind variance (kinetic energy) of the anomaly are counted for this index. The result shows larger anomalies in winter and relatively smaller anomalies in summer. Among those, January and February 1989 (see Figs. 3 and 4) are the largest, indicating the most unusual months during the last 50 years.

Although the anomaly norm so defined contains the fundamental information on the abnormality, it may be more appropriate to normalize it by the climatological mean value for every month to remove the seasonal change. The normalized anomaly norm, $E_A/\bar{E}_A$, is referred to as an abnormality index for the atmosphere in this study. Figure 7 illustrates the abnormality index of the barotropic component of the atmosphere for 1953 to 2002. The abnormality index varies around the mean of unity. The probability distribution of the variation may be regarded as Chi-squared distribution with the estimated degree of freedom of 28. The degree of freedom is estimated from the calculated mean and variance (see Jenkins and

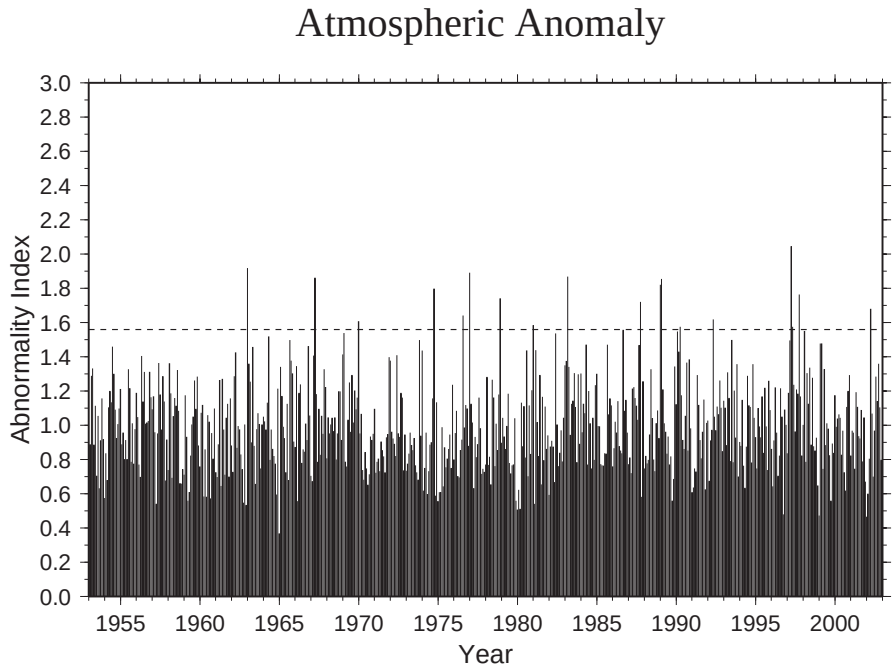

Fig. 7. The abnormality index of the barotropic component of the atmosphere $E_A/\tilde{E}_A$ for 1953 to 2002. The dashed line denotes the top 3% level of the probability.

Watts 1968). The abnormality index thus represents the Chi-squared value normalized by the degree of freedom. The abnormal month may be defined by the probability of the top 3% of the Chi-squared distribution, which corresponds to 1.56 and above in this case. According to the result, April 1997 (see Fig. 5) appears to be the most abnormal month during the last 50 years exceeding the months of January and February 1989. The abnormality index reaches to 2.04. The probability of this Chi-squared value corresponds to one in 1000 events. The abnormality index of the atmosphere for the top 18 abnormal months (top 3%) during the last 50 years for 1953 to 2002 is listed in Table 1.

4.2 Anomaly norm for the external forcing

The same analysis of the quantification for the abnormal forcing anomaly is conducted in this subsection. The magnitude of the forcing anomaly can be measured by the same 2-norm as (11) replacing w_i' by s_i'. The forcing anomaly norm E_F is thus defined by the following dimensionless form:

$$E_F = \sum_i \frac{1}{2} |s_i'|^2. \tag{12}$$

The value must be divided by 2 for zonal components as before.

Figure 8 shows the time series of the forcing anomaly norm E_F for 1953 to 2002. The result shows larger anomalies in winter and relatively smaller anomalies in summer as in Fig. 6. Among those, January 1963, February 1983 and January 1984 are the largest, indicating the most unusual months with respect to the forcing during the last 50 years. January 1963 is one of the most abnormal month as discussed in Fig. 1. The winter of 1982/83 corresponds to the El Niño year, although 1983/84 is not. January and February 1989 (see Figs. 3 and 4) are also large, suggesting a strong link with the abnormal winter associated with La Niña discussed in section 3.3.

The raw value of the forcing anomaly norm in Fig. 8 is normalized as before by the climatological mean value for every month to remove the seasonal change. The number $E_F/\tilde{E}_F$ is referred to as the abnormality index for the forcing. Figure 9 illustrates the abnormality index of the forcing for 1953 to 2002. The probability distribution of the variation may be regarded as Chi-squared distribution with the estimated degree of freedom of 49. The abnormality index

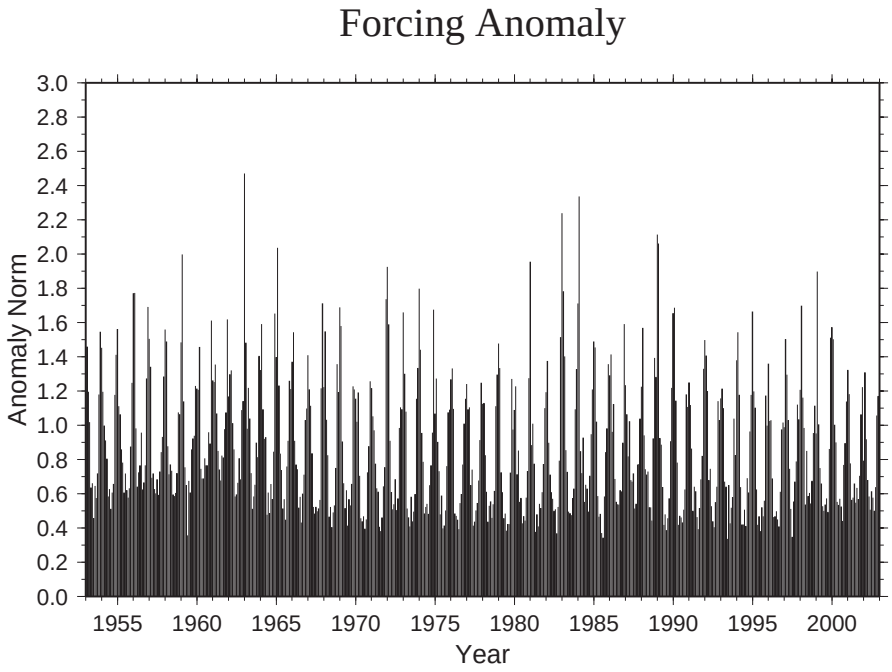

Fig. 8. The anomaly norm of the forcing to the barotropic component of the atmosphere E_F (10^{-7}) for 1953 to 2002.

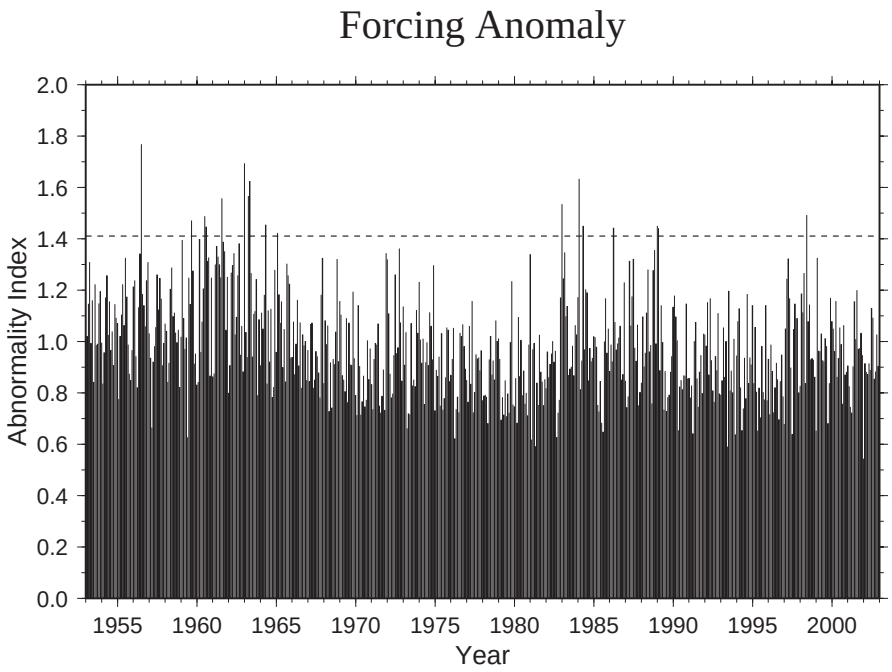

Fig. 9. The abnormality index of the forcing to the barotropic component of the atmosphere $E_F/\tilde{E}_F$ for 1953 to 2002. The dashed line denotes the top 3% level of the probability.

represents the Chi-squared value normalized by the degree of freedom. The larger degree of freedom of forcing than state variables indicates that the forcing variation is much closer to the normal distribution. The abnormal month may be defined by the probability of the top 3% of the Chi-squared distribution, which corresponds to 1.41 and above in this case. According to the result, July 1956 appears to be the most unusual month during the last 50 years. The abnormality index reaches to 1.77. The probability of this Chi-squared value corresponds to one in 1000 events. The well-known abnormal weather of January 1963 is the second, and the abnormality index is 1.69. February 1984 exceeds January 1983 of the El Niño winter by the normalization. January and February 1989 are also large, showing the index of 1.45. The abnormality index of the forcing for the top 18 abnormal months (top 3%) during the last 50 years for 1953 to 2002 is listed in Table 1.

Table 1. A list of the most abnormal year, month and its abnormality index, measured by the atmospheric anomaly w_i' and forcing anomaly s_i' for the barotropic component of the atmosphsere during the 50 years from 1953 to 2002. The abnormality index represents the anomaly 2-norm scaled by its mean value. The asterisc denotes the month when both atmospheric anomaly and forcing anomaly are listed in the table.

Atmospheric Anomaly				Forcing Anomaly		
1	1997	4	2.04	1956	7	1.77
2	1963	1	1.92*	1963	1	1.69*
3	1977	1	1.89	1984	2	1.63
4	1983	3	1.87	1963	5	1.62
5	1967	4	1.86	1963	4	1.57
6	1989	2	1.86*	1961	8	1.56
7	1989	1	1.82*	1983	1	1.53
8	1974	10	1.80	1998	6	1.49
9	1997	10	1.76	1960	7	1.49
10	1978	12	1.74	1959	9	1.47
11	1987	10	1.72	1964	5	1.45
12	2002	4	1.68	1989	1	1.45*
13	1976	8	1.64	1984	5	1.45
14	1992	5	1.62	1960	8	1.45
15	1970	1	1.61	1989	2	1.44*
16	1981	1	1.58	1986	4	1.44
17	1997	5	1.58	1965	2	1.42
18	1990	4	1.57	1960	3	1.40

4.3 Anomaly norm for the SST

Finally, the same analysis is conducted for the quantification of the abnormal SST anomaly in this subsection. The magnitude of the overall SST anomaly is measured by the 2-norm of the SST anomaly integrated over the area S of the ocean.

$$E_S = \int_S |SST'|^2 \, dS. \tag{13}$$

The anomaly norm so defined is normalized as before by the climatological mean value for every month to remove the seasonal change. The number $E_S/\tilde{E}_S$ is referred to as the abnormality index for the SST.

Figure 10 illustrates the time series of the abnormality index of the SST anomaly for 1953 to 2002. Although the result is presented for 50 years, the first half of the period before 1979 will not be argured much due to the quality problem in data. The result shows two major El Niño events for 1982/83 and 1997/98. Quantitatively, the abnormality index of the El Niño event for 1997/98 is 3.6, which is clearly larger than 2.6 for 1982/83. In addition to these two extreme events, high indices are seen for summer of 1987 and for spring of 1992. The latter may corresponds to the major volcanic eruption of Mt. Pinatubo. The abnormality index shows approximately 5 year period, and is uneasy to fit with Chi-squared distribution. The La Niña event for 1988/89 is expressed by rather weak signal with this measure.

It is interesting to compare the abnormality index for the SST in Fig. 10 with those for the atmosphere and forcing in Figs. 7 and 9. The extreme events in the SST show persistency to the extent of about one year. Despite the persistent impact of the SST, the atmosphere and its forcing field respond rather randomly with the time scale of a month. Therefore, some atmospheric extreme events correspond to the extreme SST event, but some show no correspondence even for the same SST anomaly. The short time scale of the atmospheric extreme events may represent the dominant influence of the natural variability contained in the nonlinear 2-D fluid dynamics of the barotropic component of the atmosphere.

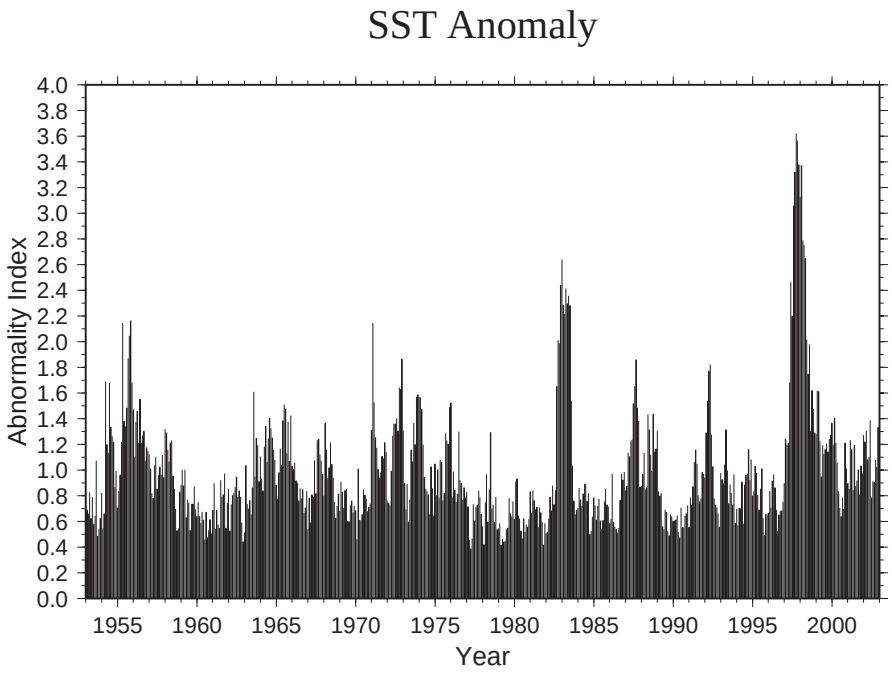

Fig. 10. The abnormality index of the SST anomaly $E_S/\tilde{E}_S$ for 1953 to 2002.

4.4 Scatter diagram of the anomaly indices

The separation of the atmospheric extreme events in a group of the pure natural variability of the atmosphere and in a group under the strong constraint of the external forcing may be an important research subject for the understanding of the cause of the abnormal weather. An attempt to answer to that question is conducted in this subsection by plotting the scatter diagram of the abnormality indices for the atmosphere and its forcing.

The 18 top most extreme events (top 3%) during the 50 years from 1953 to 2002 are listed in Table 1 in the order of the abnormality score for both the atmospheric and forcing anomalies. As discussed in section 4.1, the most extreme event was April 1997 (see Fig. 5) with the abnormality score of 2.04. The Chi-squared probability of this score is one in 1000 events. January 1963 (Fig. 1) discussed in section 3.1 appears to be second, and January 1977 (Fig. 2) discussed in section 3.2 appears to be third. According to the list, February and January 1989 (Figs. 3 and 4) are ranked as the 6th and 7th abnormal months in the historical record.

On the other hand, the most extreme forcing occurs in July 1956 with the abnormality score of 1.77. Since the data is rather old, we avoid discussing in detail. January 1963 (Fig. 1) as discussed in section 3.1 appears to be second. January and February 1989 (Figs. 3 and 4) are ranked as the 12th and 15th abnormal months in the historical record. The months appearing in both columns are marked by asterisks, which include January 1963, January, and February 1989.

Figure 11 presents the scatter diagram of the abnormality indices for the atmosphere (abscissa) versus that for the forcing (ordinate) for 50 years from 1953 to 2002. The correlation between the two abnormality indices is 0.48 which is statistically significant at 99% level. The result implies that the atmospheric anomaly norm is large when the forcing anomaly norm is large, suggesting that the extreme forcing certainly shifts the likelihood of the extreme barotropic anomaly. Since the anomaly norm is normalized by its mean value, abnormality of 1.0 represents the usual state. On the other hand, the value of 0.0 represents that the state coincides with the climate. It is found that such a quite normal state has never happened in the record. This may be another important finding in itself to understand the nature of

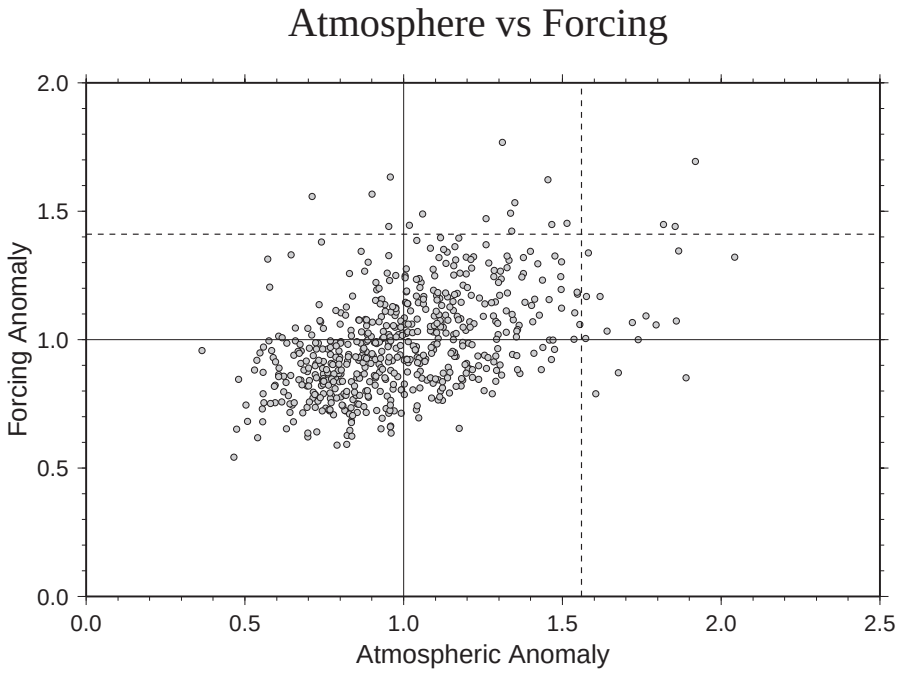

Fig. 11. The scatter diagram of the abnormality indices for the atmosphere (abscissa) versus that for the forcing (ordinate) for 50 years from 1953 to 2002. The dashed lines denote the top 3% level of the probability. The numbers of the extreme (and non-extreme) events separated by the dashed lines in the figure are 3, 14, 568, and 15, respectively, for each quadrant.

the variability of the atmosphere. The large values of the abnormality index correspond to the abnormal or extreme events both for the atmosphere and forcing with different degree of freedoms. The dashed line at 1.56 for the atmospheric anomaly represents 3% Chi-squared probability for the threshold of the abnormal events. In fact, 18 extreme events are counted beyond this threshold out of the total of 600 samples as listed in Table 1. The other dashed line at 1.41 for the forcing anomaly represents 3% Chi-squared probability for the threshold of the abnormal events, and 17 extreme events are counted here. The numbers of the extreme (and non-extreme) events separated by the dashed lines in Fig. 11 are 3, 14, 568, and 15, respectively, for each quadrant.

According to the distribution in Fig. 11, it is noteworthy that only 3 events appear at the corner of the extreme events for both indices. These include the month of January 1963, January and February 1989 as listed in Table 1 with the symbol of asterisks. Those months are likely to be abnormal because the external forcing was abnormal, although more careful analysis of the horizontal pattern may be needed to conclude it. Interestingly, 15 out of 18 extreme events of the atmosphere are associated with non-extreme external forcing. The result suggests that more than 83% of the abnormal weather are induced by the natural variability of the atmosphere with "non-extreme" external forcing. Likewise, 14 out of 17, i.e., more than 82% of the extreme forcing result in non-extreme atmosphere. The result implies that the external forcing is the secondary importance for the occurrence of the abnormal weather, which, in turn, emphasize the importance of the natural variability of the barotropic component of the atmosphere.

5. Summary and conclusions

In this study, recent extreme events are analyzed in the dynamical framework of the barotropic component of the atmosphere. Most of the extreme events are induced by the low-frequency variabilities such as blocking high, Arctic Oscillation (AO) and PNA-like teleconnections, which are characterized by their barotropic structure. Therefore, the dynamical

understanding of those low-frequency variabilities under the constraint of the 2-D fluid mechanics may be the key problem for the solution. We attempted to separate the cause of the extreme events in a natural variability of the 2-D fluid dynamics and/or a forced response to the external forcing of the barotropic component of the atmosphere. The SST anomaly is also investigated to compare with the external forcing anomaly.

The magnitude of the anomaly of the atmosphere is measured by the energy norm of the anomaly integrated over the Northern Hemisphere. The abnormality index is then defined by normalizing the energy norm by its climate value. According to the result of the analysis, the most abnormal month during the recent 50 years from 1953 to 2002 was April 1997 with the abnormality score of 2.04. The probability of the Chi-squared value corresponds to one in 1000 events. January 1963 appears to be second, and January 1977 appears to be third. February and January 1989 are ranked as the 6th and 7th abnormal months in the historical record. It is shown that January 1963, February and January 1989 are associated with abnormal external forcing to the barotropic component of the atmosphere. In this regard, those months are likely to be abnormal because the external forcing was abnormal, although more careful analysis of the horizontal pattern may be needed to conclude it.

It is found in this study that more than 80% of the abnormal weather are induced by the natural variability of the atmosphere with "non-extreme" external forcing, as long as the barotropic component is concerned. Likewise, more than 80% of abnormal external forcing result in non-extreme weather. The result implies that the external forcing is the secondary importance for the occurrence of abnormal weather, which, in turn, emphasize the importance of the natural variability of the barotropic component of the atmosphere for the monthly mean time scale.

The abnormality indices of the barotropic atmosphere and its forcing are compared with that of the SST. The extreme events of the SST show persistency to the extent of about one year. Despite the persistent impact of the SST, the atmosphere and its forcing field respond rather randomly with the time scale of a month. Therefore, some atmospheric extreme events correspond to the extreme SST event, but most of the atmospheric extreme events show no correspondence to the same SST anomaly. The short time scale of the atmospheric extreme events may represent the dominant influence of the natural variability contained in the nonlinear 2-D fluid dynamics of the barotropic component of the atmosphere.

The conclusion derived by this study suggests the importance of the dynamical understanding of the barotropic component of the atmosphere for the improvement of the medium to long-range forecasting. Although the importance of the natural variability has been concluded, some extreme events could be more closely related to forcing if the analysis is conducted in specific subregions such as a single continent or single ocean. Some extreme events could also have been induced by smaller norm of forcing anomaly, but a specific pattern. Those problems are reserved as the subject of future work.

Acknowledgments

The authors would like to express acknowledgments to Professors T. Yasunari, F. Kimura, and H. Ueda for their valuable suggestion and advice. Thanks are also due to Dr. John Walsh of IARC/UAF for his constructive comments. The authors appreciate Ms. K. Honda for her technical assistance. The research was partly supported by Asahi Breweries Foundation.

References

Bell, G.D. and M.S. Halpert, 1998: Climate assessment for 1997. *Bull. Amer. Meteor. Soc.*, **79**, (May) S1–S50.

———, ———, C.F. Ropelewski, V.E. Kousky, A.V. Douglas, R.C. Schnell, and M.E. Gelman, 1999: Climate assessment for 1998. *Bull. Amer. Meteor. Soc.*, **80**, (May) S1–S48.

Branstator, G., 1990: Low-frequency patterns induced by stationary waves. *J. Atmos. Sci.*, **47**, 629–648.

——— and J. Frederiksen, 2003: The seasonal cycle of interannual variability and the dynamical imprint of the seasonally varying mean state. *J. Atmos. Sci.*, **60**, 1577–1592.

Frederiksen, J. and G. Branstator, 2001: Seasonal and intraseasonal variability of large-scale barotropic modes. *J. Atmos. Sci.*, **58**, 50–69.

Graf, H.-F., J. Perlwitz, and I. Kirchner, 1994: Northern Hemisphere tropospheric mid-

latitude circulation after violent volcanic eruptions. *Beitr. Phys. Atmos.*, **67**, 3–13.

Graham, N.E., 1994: Decadal-scale climate variability in the tropical and north Pacific during the 1970s and 1980s: Observations and model results. *Clim. Dyn.*, **10**, 135–162.

IPCC (Intergovernmental Panel on Climate Change), 2001: *Climate Change 2001, The Scientific Basis*. Eds. Houghton, J.T., Y. Ding, D.J. Griggs, M. Noguer, P.J. van der Linden, X. Dai, K. Maskell, and C.A. Johnson. Cambridge University Press. 881 pp.

Jenkins, G.M. and D.G. Watts, 1968: *Spectral Analysis and its Application*. Holden-Day, 525 pp.

JMA, 1994: *Abnormal Weather Report 1994*. Japan Meteorological Agency, 444 pp (in Japanese).

———, 1999: *Abnormal Weather Report 1999*. Japan Meteorological Agency, 341 pp (in Japanese).

Kalnay, E.M. and Coauthors, 1996: The NCEP/NCAR reanalysis project. *Bull. Amer. Meteor. Soc.*, **77**, 437–471.

Kasahara, A., 1976: Normal modes of ultralong waves in the atmosphere. *Mon. Wea. Rev.*, **104**, 669–690.

———, 1977: Numerical integration of the global barotropic primitive equations with Hough harmonic expansions. *J. Atmos. Sci.*, **34**, 687–701.

———, 1978: Further studies on a spectral model of the global barotropic primitive equations with Hough harmonic expansions. *J. Atmos. Sci.*, **35**, 2043–2051.

Kashiwabara, T., 1987: On the recent winter cooling in the north Pacific. *Tenki*, **34**, 777–781 (in Japanese).

Kawamata, M., S. Yamada, T. Kudoh, K. Takano, and S. Kusunoki, 1992: Atmospheric temperature variation after the 1991 Mt. Pinatubo volcanic eruption. *J. Meteor. Soc. Japan*, **70**, 1161–1166.

Kraichnan, R.H., 1967: Inertial ranges in two-dimensional turbulence. *Phys. Fluids*, **10**, 1417–1423.

Kravtsov, S., A.W. Robertson, and M. Ghil, 2003: Low-frequency variability in a baroclinic beta channel with land-sea contrast. *J. Atmos. Sci.*, **60**, 2267–2293.

Kushnir, Y., W.A. Robinson, I. Blade, N.M.J. Hall, S. Peng, and R. Sutton, 2002: Atmospheric GCM response to extratropical SST anomalies: Synthesis and evaluation. *J. Climate*, **15**, 2233–2256.

Lengaigne, M., J.P. Boulanger, C. Menkes, G. Madec, P. Delecluse, E. Guilyardi, and J. Slingo, 2003: The March 1997 westerly wind event and the onset of the 1997/98 El Niño: Understanding the role of the atmospheric response. *J. Climate*, **16**, 3330–3343.

Namias, J., 1978: Multiple causes of the North American abnormal winter 1976–77. *Mon. Wea. Rev.*, **106**, 279–295.

Nitta, T. and S. Yamada, 1989: Recent warming of tropical sea surface temperature and its relationship to the Northern Hemisphere circulation. *J. Meteor. Soc. Japan*, **67**, 375–383.

Peng, S., W.A. Robinson, and S. Li, 2003: Mechanism for the NAO response to the north Atlantic SST tripole. *J. Climate*, **16**, 1987–2004.

Smith, T.M. and R.W. Reynolds, 2003: Extended reconstruction of global sea surface temperatures based on COADS data (1854–1997). *J. Climate*, **16**, 1495–1510.

Tanaka, H.L., 1985: Global energetics analysis by expansion into three dimensional normal mode functions during the FGGE winter. *J. Meteor. Soc. Japan*, **63**, 180–200.

———, 1998: Numerical simulation of a life-cycle of atmospheric blocking and the analysis of potential vorticity using a simple barotropic model. *J. Meteor. Soc. Japan*, **76**, 983–1008.

———, 2003a: The review of the dynamics of the low-frequency variability and its predictability. *Gross Wetter, JMA*, **41**, 51–88 (in Japanese).

———, 2003b: Analysis and modeling the Arctic Oscillation using a simple barotropic model with baroclinic eddy forcing. *J. Atmos. Sci.*, **60**, 1359–1379.

——— and M.F. Milkovich, 1990: A heat budget analysis of the polar troposphere in and around Alaska during the abnormal winter of 1988/89. *Mon. Wea. Rev.*, **118**, 1628–1639.

——— and D. Nohara, 2001: A study of deterministic predictability for the barotropic component of the atmosphere. *Sci. Rep., Inst. Geosci., Univ. of Tsukuba*, **22A**, 1–21.

Thompson, D.W.J. and J.M. Wallace, 1998: The arctic oscillation signature in the wintertime geopotential height and temperature fields. *Geophy. Res. Let.*, **25**, 1297–1300.

Trenberth, K.E., 1990: Recent observed interdecadal climate change in the Northern Hemisphere. *Bull. Amer. Meteor. Soc.*, **71**, 988–993.

——— and J.W. Hurrell, 1994: Decadal atmosphere-ocean variations in the Pacific. *Clim. Dyn.*, **9**, 303–319.

Tung, K.K. and W.W. Orlando, 2003: The k^{-3} and $k^{-5/3}$ energy spectrum of atmospheric turbulence: Quasi-geostrophic two-level model simulation. *J. Atmos. Sci.*, **60**, 824–835.

Wallace, J.M. and M.L. Blackmon, 1981: Observations of low-frequency atmospheric variability. *Large-scale Dynamical Processes in the Atmosphere*, B.J. Hoskins and R.P. Pearce, Eds., Academic Press, 55–94.

——— and D.S. Gutzler, 1981: Teleconnections in the geopotential height field during the Northern Hemisphere Winter. *Mon. Wea. Rev.*, **109**, 784–812.

Walsh, J. and W.L. Chapman, 1990: Shour-term climate variability of the Arctic. *J. Climate*, **3**, 237–250.

Wiin-Nielsen, A. and M. Drake, 1965: On the energy exchange between the baroclinic and barotropic components of atmospheric flow. *Mon. Wea. Rev.*, **93**, 79–92.

———, 1967: On the annual variation and spectral distribution of atmospheric energy. *Tellus*, **19**, 540–559.

Yasunari, T., 1997: Analysis of the abnormal weather of the summers in 1993/1994. *Meteor. Res. Notes.* 290 pp (in Japanese).